# Alternative splicing of the rat $Ca_v3.3$ T-type calcium channel gene produces variants with distinct functional properties[1]

Janet Murbartián[a], Juan Manuel Arias[a], Jung-Ha Lee[b], Juan Carlos Gomora[c], Edward Perez-Reyes[a,*]

[a] *Department of Pharmacology, University of Virginia, P.O. Box 800735, 1300 Jefferson Park Avenue, Charlottesville, VA 22908-0735, USA*
[b] *Department of Life Science, Sogang University, Shinsu-dong, Mapo-gu, Seoul 121-742, South Korea*
[c] *Departamento de Biofísica, Instituto de Fisiología Celular, UNAM, México D.F. 04510, Mexico*

Received 29 July 2002; accepted 9 August 2002

First published online 5 September 2002

Edited by Maurice Montal

**Abstract Molecular diversity in T-type $Ca^{2+}$ channels is produced by expression of three genes, and alternative splicing of those genes. Prompted by differences noted between rat and human $Ca_v3.3$ sequences, we searched for splice variants. We cloned six variants, which are produced by splicing at exon 33 and exon 34. Expression of the variants differed between brain regions. The electrophysiological properties of the variants displayed similar voltage-dependent gating, but differed in their kinetic properties. The functional impact of splicing was interrelated, suggesting an interaction. We conclude that alternative splicing of the $Ca_v3.3$ gene produces channels with distinct properties.** 

*Key words:* Calcium channel; T-type; Gene; Alternative splicing; Electrophysiology; Rat; Brain

## 1. Introduction

T-type calcium channels are thought to play important roles in neuronal activity, including activation of low-threshold spikes that lead to burst firing [1]. Molecular cloning and expression studies have established the existence of three genes encoding T-type channels. The third member of this family, $Ca_v3.3$ (formerly $\alpha1I$), has been cloned from both rat and human sources [2–4]. Although all three $Ca_v3$ channels are low voltage-activated, some studies have found that the voltage dependence of activation and inactivation of $Ca_v3.3$ channels occurs at slightly more positive potentials [2,5,6]. Although the properties of recombinant $Ca_v3.3$ $\alpha1$ subunits expressed alone in 293 cells are slower than most native T-type currents, similar kinetics have been described for T-type currents in neurons isolated from the lateral habenula [7], retina [8], and laterodorsal [9] and reticular nucleus of the thalamus [10]. Prominent expression of $Ca_v3.3$ mRNA has been detected in many of these brain regions [11], suggesting that $Ca_v3.3$ channels mediate these currents. Slow T-type currents are thought to play an important role in sustained neuronal firing [5,10].

Alignment of rat and human $Ca_v3.3$ sequences led to the suggestion that there were either cloning and/or errors in the rat sequence that produced shifts in the reading frame [4]. We have re-investigated the structure of the rat $Ca_v3.3$, and now report the existence of alternative splice variants that encode distinct carboxy-termini. These results indicate that the $Ca_v3.3$ gene is alternatively spliced in a brain region-specific manner, producing functionally distinct channels.

## 2. Materials and methods

### 2.1. Cloning of $Ca_v3.3$ cDNAs

A rat brain λgt10 cDNA library (Clontech, Palo Alto, CA, USA) was screened using nucleotides (nt) 5143–6197 of rat $Ca_v3.3$ (GenBank accession number AF086827 [2]). DNA sequences were determined at the University of Virginia Biomolecular Research Facility.

### 2.2. RNA isolation and RT-PCR

Total RNA was extracted from rat whole brain or indicated regions (kindly donated by Dr. E. Talley). cDNA was synthesized from 1 μg total RNA with 5 μM random decamers, 0.5 mM each dNTP, 100 U M-MLV reverse transcriptase, and 20 U SUPERase·In™ (Ambion, Austin, TX, USA). Amplification reactions were performed in a Mastercycler gradient (Eppendorf, Westbury, NY, USA) and contained 2.5 μl cDNA, 0.4 μM each primer, 0.8 mM dNTPs and 0.6 U *Taq* DNA polymerase (Eppendorf). After a 150 s denaturation step, reactions were cycled 35 times using 25 s for denaturation (94°C) and annealing (62°C), and ~60 s/kb for extension (72°C). PCR products were cloned with the pCRII-TOPO kit (Invitrogen, Carlsbad, CA, USA). PCR primers were 21 nt long, and reported positions refer to GenBank accession number AF086827. Full-length Δ33 variants were cloned using overlapping extension PCR and *Vent* DNA polymerase (New England Biolabs, Beverly, MA, USA). Full-length cDNAs of each variant were constructed in two steps using fragments generated by *Hin*dIII (3386), *Spe*I (5228), *Bsp*EI (5571), and *Eco*RI (polylinker).

### 2.3. Electrophysiology

293 cells (human embryonic kidney, #CRL-1573, American Type Culture Collection, Manassas, VA, USA) were transiently transfected by the calcium phosphate method with plasmid DNAs encoding each $Ca_v3.3$ variant and green fluorescent protein (5:1 ratio). Electrophysiological experiments were carried out using the whole cell configuration of the patch clamp technique as described previously [12]. Whole cell $Ca^{2+}$ currents were recorded using the following external solution (in mM): 5 $CaCl_2$, 155 tetraethyl ammonium (TEA) chloride, and 10 HEPES, pH adjusted to 7.4 with TEA-OH. The internal pipette solution contained the following (in mM): 125 CsCl, 10 EGTA, 2 $CaCl_2$, 1 $MgCl_2$, 4 Mg-ATP, 0.3 $Na_3GTP$, and 10 HEPES, pH adjusted to 7.2 with CsOH. Series resistance values ranged between 2 and 8 MΩ ($4.4 \pm 0.2$, $n = 113$) and were compensated between protocols to at least 70%. Average cell capacitance was $11.6 \pm 0.6$ pF ($n = 113$). The holding potential was −100 mV. All experiments

*Corresponding author. Fax: (1)-434-982 3878.
*E-mail address:* eperez@virginia.edu (E. Perez-Reyes).

[1] The sequences reported herein have been assigned GenBank accession numbers AY128644–AY128648.

0014-5793/02/$22.00 © 2002 Published by Elsevier Science B.V. on behalf of the Federation of European Biochemical Societies.
PII: S0014-5793(02)03341-0

were performed at room temperature (~22°C). Average data are presented as mean ± S.E.M. The results were obtained from 56 transfections, and each construct was tested in at least four transfections. Statistical tests included unpaired two-tailed Student's *t*-test for comparing two data sets, and the *F*-test for comparing two models such as single or double exponential fits.

## 3. Results and discussion

### 3.1. Cloning

Alignment of the rat and human $Ca_v3.3$ sequences indicated that there were shifts in the reading frame in the region encoding the carboxy-terminus [4]. As reported previously [6], resequencing of the original rat $Ca_v3.3$ cDNA did not reveal any errors that would explain the shorter carboxy-terminus (Fig. 1A). Since the frame shift occurs at an intron/exon border of the human gene, we searched for alternatively spliced variants. A rat brain cDNA library was screened, and five recombinants were purified, subcloned, and sequenced. Comparison of their sequences to the rat $Ca_v3.3a$ sequence revealed the presence of two variants spliced at nt 5473. The sequence of clone 6 contained 40 additional nucleotides not found previously, while that of clone 2 contained 121 additional nucleotides. We refer to the original rat clone as $Ca_v3.3a$, the clone 6 variant as $Ca_v3.3b$, and the clone 2 variant as $Ca_v3.3c$. The deduced amino acid sequences of these clones were aligned to the human $Ca_v3.3$ (Fig. 1A). Although the nucleotide sequences of all three variants are identical after the variant region, $Ca_v3.3a$ is in a different reading frame from either $Ca_v3.3b$ or c, leading to a short carboxy-terminus. In contrast, $Ca_v3.3b$ has a long carboxy-terminus that is of similar length, and shares 85% identity, with the full-length human $Ca_v3.3$. $Ca_v3.3c$ contains 40 additional amino acids, but is otherwise identical to $Ca_v3.3b$. The rat a, b, and c isoforms differ at the analogous position as the exon 33–34 border in the human gene, indicating that these variants are produced by splicing to alternative 3′ acceptor sites in exon 34 (Fig. 1B).

To determine the abundance and distribution of these $Ca_v3.3$ variants, we designed PCR primers that flanked this variant region (forward primer r4 at nt 5214, reverse primer r7 at nt 5505). The forward primer was located 5′ to exon 33, which has been reported to be alternatively spliced in human [13]. If splicing of the two sites is independent, then six products are expected. PCR amplification of rat total brain cDNA generated multiple DNA fragments of the expected sizes (Fig. 2A). The products were cloned, mapped by restriction enzymes, and representative clones were sequenced. Variants were identified that encode a, b, and c isoforms that either excluded (referred to as Δ33) or included the 5′ end of exon 33. Since each variant produces a uniquely sized PCR product (except for $Ca_v3.3a$ and Δ33b; Fig. 2B), their expression can be detected after agarose gel electrophoresis. Because the annealing sites of the PCR primers are common among all variants, product formation should only depend on the amount

**A**

```
                                                    ∇ Exon 33
Cav3.3          RLPTSSPGAPGRGSGGAGAGGDTESHLCRHCYSPAQ ETLWLDSVSLIIKDSLEGELTIIDNLSGSVFHHYASPDG  1815
Cav3.3-Δ33      RLPTSSPGAPGRGSGGAGAGGDTESHLCRHCYSPAQ ------------DSLEGELTIIDNLSGSVFHHYASPDG  1802
Human Cav3.3    RLPTgSPGAPGRGSGGAGgGGDTEggLCRHCYSPAQ EnLWLDSVSLIIKDSLEGELTIIDNLSGSiFHHYsSPaG  1803

                          ∇ Exon 34
Cav3.3a         CGKCHHDKQE TGLHPSCWGMT @                                                      1835
Cav3.3b         CGKCHHDKQE ----------------------------VQLAETEAFSLNSDRSSSILLGDDLSLEDPTACPQGPK  1863
Cav3.3c         CGKCHHDKQE GPVAQRSRPRLPHPSPRVTRGHHLPLQVQLAETEAFSLNSDRSSSILLGDDLSLEDPTACPQGPK  1890
Human Cav3.3    CkKCHHDKQE ----------------------------VQLAETEAFSLNSDRSSSILLGDDLSLEDPTACPpGRK  1851

                     ∇ Exon 35                                                ∇ Exon 36
Cav3.3bc        ESK GELEPPEPMQAGDLDECFFPFASEPVSTGPESLLCEMGAIPFNPVQSWLKHESSQ APQSPFSPDGSSPLLQM  1938
Human Cav3.3    dSK GELdPPEPMrvGDLDECFFPlsSEaVSpdPEnfLCEMeeIPFNPVrSWLKHdSSQ APpSPFSPDaSSPLLpM  1926

                                                              ∇ Exon 37
Cav3.3bc        PAEFFHPAVSASQKGQEPGMSAGTLPKIALQGSWASLRSPSVNCTLLRQ ATVSDTSLDASPSSSAGSLQTTLEDS  2013
Human Cav3.3    PAEFFHPAVSASQKGpEkGtgtGTLPKIALQGSWASLRSPrVNCTLLRQ ATgSDTSLDASPSSSAGSLQTTLEDS  2001

Cav3.3bc        LTLSDSPRRALGPPVQVPGPRASLSPATRRRLSLRGRGLFSLRGLRAHQRSHSSGGSTSPGCTHHDSMDPSDEEG  2088
Human Cav3.3    LTLSDSPRRALGPPapaPGPRAgLSPAaRRRLSLRGRGLFSLRGLRAHQRSHSSGGSTSPGCTHHDSMDPSDEEG  2076

Cav3.3bc        RGGAGGGGAGSEHSETLSSLSLTSLFCLPPTLPPPGLTPARKFNSTSSLAAGPGRPGSTVSARGLVRSPSWAADR  2163
Human Cav3.3    RGGAGGGGAGSEHSETLSSLSLTSLFCpPPtlPaPGLTPARKFsSTSSLAA-PGRPhaaalAhGLaRSPSWAADR  2150

Cav3.3bc        SKDPPGQAQLVSGLGSSAPGPQPPPGE--STDAASKRKR @                                     2199
Human Cav3.3    SKDPPGrApLpmGLGplAPpPQPlPGElepgDAASKRKR @                                     2188
```

**B**

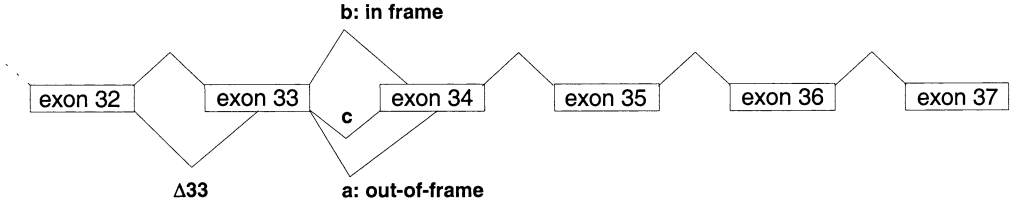


Fig. 1. Carboxy-terminal splice variants of $Ca_v3.3$. A: Deduced amino acid sequences of rat $Ca_v3.3$ variants are aligned to the full-length human $Ca_v3.3$ (GenBank accession number AF393329 [12]). Intron/exon borders of the human gene are marked (▽) [12,13]. Identical amino acids are shown in uppercase in the human sequence. B: Diagrammatic representation of splicing events.

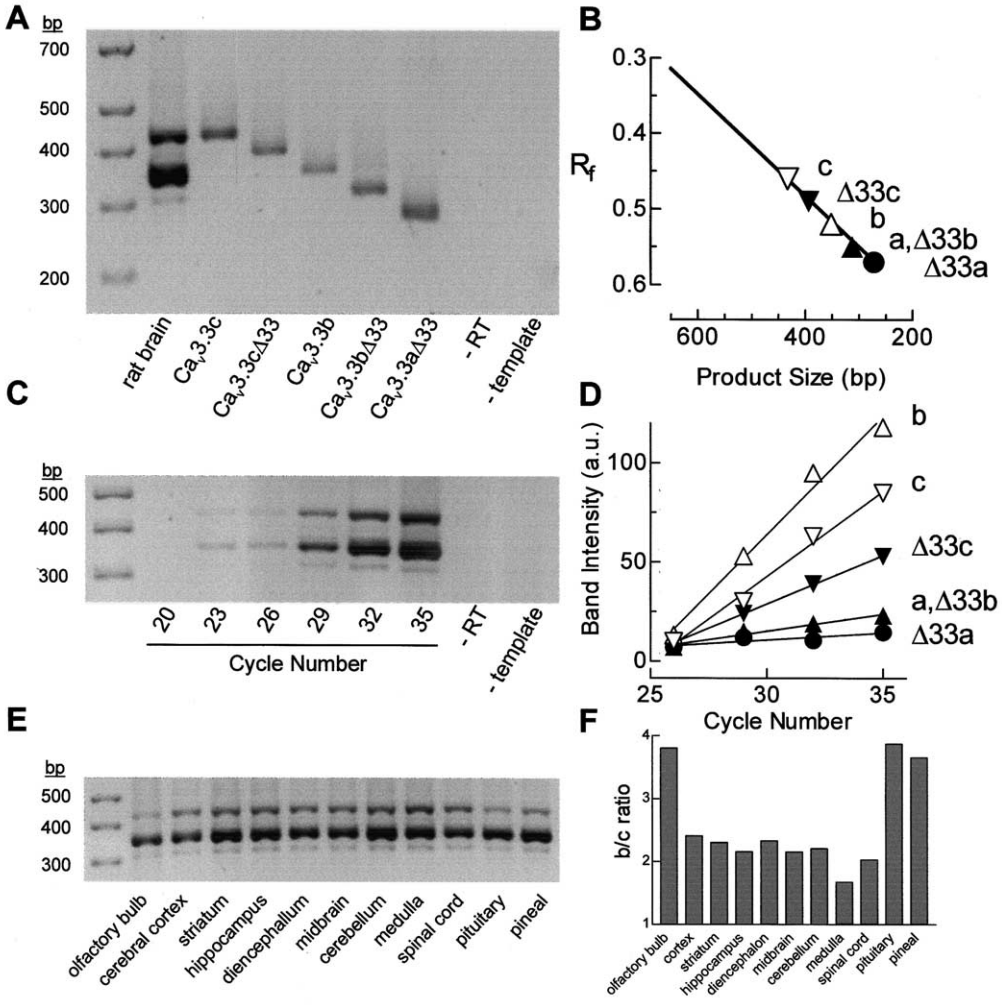


Fig. 2. Expression and distribution of the rat $Ca_v3.3$ splice variants. Ethidium bromide-stained agarose gels showing RT-PCR products amplified from rat total brain RNA using primers r4 and r7 (A,C,E). To correlate the bands amplified from rat brain, representative plasmids were PCR amplified using the same primers. Negative controls included omission of reverse transcriptase from the cDNA synthesis reaction (−RT), and omission of cDNA to the PCR reaction (−template). B: Relative electrophoretic mobility ($R_f$) of the plasmid PCR products. C: Agarose gel of RT-PCR products obtained by varying the number of cycles. D: PCR products shown in C were quantitated using the histogram function in Adobe Photoshop 5.0 (Adobe Systems, San Jose, CA, USA). The band intensity in arbitrary units (a.u.) was plotted versus cycle number and fit by linear regression. E: PCR products amplified from various regions of rat brain. F: Ratio of $Ca_v3.3$b and c variants in each brain region.

of starting material and the number of cycles. Analysis of PCR reactions run for varying cycles demonstrated that product formation was linear between 25 and 35 cycles (Fig. 2C,D), indicating that the intensity of ethidium bromide-stained bands correlated with the abundance of the mRNA encoding each variant. Other quantitative methods would have met with limited success because there are many products (Q-PCR) of similar size (RNase protection assays). Therefore, we used 35 cycles to assay cDNA prepared from various rat brain regions. The major product amplified from all regions was $Ca_v3.3$b (Fig. 2E). The c isoform was detected to a lower extent in all regions, showing an even weaker expression in olfactory bulb, pituitary, and pineal gland (Fig. 2F). PCR products representing the original $Ca_v3.3$a isoform showed the weakest expression. Products representing the Δ33 variants were less abundant, indicating that splicing to the internal acceptor site occurred in less than 30% of the transcripts.

To confirm the abundance of each variant we subcloned the PCR products from total brain mRNA and characterized 52 recombinants. The observed rank order of abundance was the following: $Ca_v3.3b \gg Ca_v3.3\Delta33b \geq Ca_v3.3c > Ca_v3.3\Delta33c > Ca_v3.3\Delta33a$. The ratio of both Δ33b to b and Δ33c to c was approximately 1:4. These results are in good agreement with those of the agarose gel analysis of the PCR products.

Somewhat surprisingly none of these clones corresponded to the $Ca_v3.3$a isoform that we [2] and others have cloned [3]. Comparison of the two published rat sequences reveals 72 nucleotide differences, resulting in 32 changes in the deduced amino acid sequence. Perhaps the most significant difference was that their cDNA lacked nine base pairs, leading to the deletion of three amino acids in IIIS4. Since S4 regions are known to play a key role in sensing voltage [14], this deletion might explain why their channel gates at voltages that are 20 mV more negative than either our rat or the human

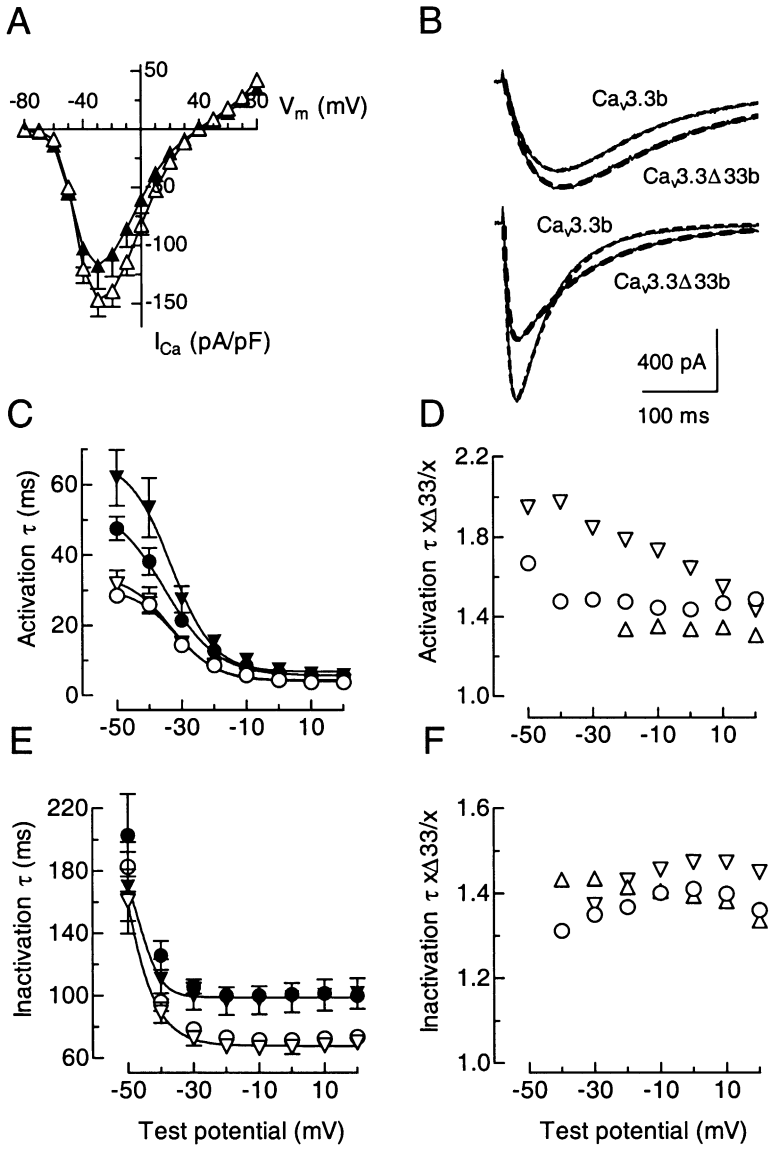


Fig. 3. Voltage-dependent gating of $Ca_v3.3$ currents. A: Current–voltage relationships of $Ca^{2+}$ currents generated by $Ca_v3.3b$ (△, $n=13$) and $Ca_v3.3\Delta33b$ channels (▲, $n=8$). B: Representative current traces from $Ca_v3.3b$ and Δ33b variants evoked by depolarizing pulses to either −50 mV (above) or −10 mV (below). Dotted lines represent the fit of the current traces with two exponentials. Activation (C) and inactivation (E) $\tau$ values are plotted as a function of test potential for $Ca_v3.3a$ (○, $n=12$), $Ca_v3.3c$ (▽, $n=11$), $Ca_v3.3\Delta33a$ (●, $n=11$), and $Ca_v3.3\Delta33c$ (▼, $n=8$). Activation (D) and inactivation (F) kinetics of each $Ca_v3.3\Delta33$ variant divided by the kinetics of its respective $Ca_v3.3$ isoform: $Ca_v3.3\Delta33a/Ca_v3.3a$, ○; Δ33b/b, △; and Δ33c/c, ▽. Only shown are data points that differed significantly ($P<0.05$).

$Ca_v3.3$ isoforms [4,12], although a contribution from the three amino acid changes in IIS4 must also be considered [3]. To test if this deletion was due to alternative splicing, we PCR amplified total rat brain cDNA with primers flanking this region (forward nt 3660, reverse nt 3730). A single product of 91 bp was detected, indicating that most transcripts contain the full IIIS4 sequence (data not shown).

PCR analysis of the human CACNA1I gene suggested the presence of an exon (#9) encoding sequences not found in rat $Ca_v3.3a$ [13]. PCR (forward nt 1282, reverse nt 1530) of this region using rat brain cDNA led to a single product, corresponding in size to the original $Ca_v3.3a$ (results not shown). As a positive control we amplified from human fetal brain cDNA and detected two transcripts of the expected size. We conclude that the rat gene is not alternatively spliced at exon 9.

### 3.2. Electrophysiology

To test the functional consequences of alternative splicing at both exons 33 and 34, full-length cDNAs were constructed that harbored all six variants. All six isoforms led to the induction of currents whose voltage dependence ($I$–$V$) was similar to low threshold-activated T-type currents (Fig. 3A; Table 1). To quantitate the voltage dependence of activation, $I$–$V$ data were normalized to the peak observed in each cell, fit with a Boltzmann equation modified to account for changes in driving force [12], then averaged. The variants had similar voltage dependence with the exception of $Ca_v3.3\Delta33b$ that gated 3 mV more negative (Table 1).

Current traces could be fit well with two exponentials, where one exponential describes channel activation, while the second describes inactivation (Fig. 3B). Activation kinetics for all variants were relatively slow at test potentials just

Table 1
Summary of electrophysiological properties of $Ca^{2+}$ currents from rat $Ca_v3.3$ channels

| | $Ca_v3.3a$ | $Ca_v3.3b$ | $Ca_v3.3c$ | $Ca_v3.3\Delta33a$ | $Ca_v3.3\Delta33b$ | $Ca_v3.3\Delta33c$ |
|---|---|---|---|---|---|---|
| Peak of *I–V* curve (mV) | −30 | −30 | −30 | −30 | −30 | −30 |
| *I* density (pA/pF) | −127 ± 17 (12) | −147 ± 14 (13) | −121 ± 23 (11) | −93 ± 14 (11) | −117 ± 20 (8) | −131 ± 23 (8) |
| Activation | | | | | | |
| $V_{1/2}$ (mV) | −41.8 ± 1.2 (12) | −42.6 ± 0.5 (13) | −41.7 ± 1.2 (11) | −42.3 ± 0.7 (11) | −45.3 ± 0.6 (8)** | −41.2 ± 0.4 (8) |
| Slope (*k*, mV) | 5.8 ± 0.3 (12) | 5.8 ± 0.2 (13) | 6.1 ± 0.3 (11) | 6.4 ± 0.3 (11) | 6.2 ± 0.2 (8) | 6.3 ± 0.2 (8) |
| Inactivation | | | | | | |
| $V_{1/2}$ (mV) | −72.4 ± 0.8 (10) | −72.6 ± 0.7 (9) | −71.3 ± 0.9 (9) | −71.2 ± 0.6 (8) | −74.4 ± 0.9 (7) | −72.6 ± 0.5 (8) |
| Slope (*k*, mV) | −5.1 ± 0.1 (10) | −5.1 ± 0.2 (9) | −5.1 ± 0.2 (9) | −5.6 ± 0.3 (8) | −5.5 ± 0.2 (7) | −6.0 ± 0.2 (8)** |
| Current kinetics at −40 | | | | | | |
| Activation ($\tau$; ms) | 25.9 ± 2.2 (12) | 33.0 ± 4.4 (13) | 27.1 ± 3.8 (11) | 38.3 ± 3.9 (11)* | 41.5 ± 7.4 (8) | 53.5 ± 8.4 (8)** |
| Inactivation rate ($\tau$; ms) | 96 ± 6 (12) | 77 ± 4 (13)** | 89 ± 7 (11) | 126 ± 9 (11)* | 111 ± 18 (8)* | 111 ± 13 (8) |
| Current kinetics at +10 | | | | | | |
| Activation ($\tau$; ms) | 3.7 ± 0.2 (12) | 3.8 ± 0.2 (13) | 4.0 ± 0.2 (11) | 5.5 ± 0.3 (11)** | 5.1 ± 0.2 (8)** | 6.2 ± 0.6 (8)** |
| Inactivation rate ($\tau$; ms) | 72 ± 2 (12) | 71 ± 4 (13) | 68 ± 4 (11) | 101 ± 4 (11)** | 98 ± 8 (8)** | 100 ± 10 (8)** |
| Deactivation kinetics at −90 (ms)[a] | 1.6 ± 0.1 (10) | 1.9 ± 0.2 (8) | 1.8 ± 0.2 (8) | 1.7 ± 0.1 (7) | 2.3 ± 0.1 (10) | 2.3 ± 0.3 (6) |
| Development of inactivation at −70 | | | | | | |
| $\tau$1 (ms) | 235 ± 58 (7) | 231 ± 56 (6) | 170 ± 30 (6) | 125 ± 58 (6) | 204 ± 46 (7) | 227 ± 41 (6) |
| $\tau$2 (s) | 1.8 ± 0.1 (7) | 1.7 ± 0.2 (6) | 1.9 ± 0.1 (6) | 1.8 ± 0.2 (6) | 2.2 ± 0.2 (7) | 2.2 ± 0.1 (6) |
| Development of inactivation at −60 | | | | | | |
| $\tau$1 (ms) | 280 ± 31 (9) | 348 ± 25 (5) | 322 ± 23 (9) | 332 ± 40 (7) | 394 ± 55 (6) | 343 ± 40 (7) |
| $\tau$2 (s) | 1.6 ± 0.1 (9) | 1.9 ± 0.3 (5) | 1.7 ± 0.1 (9) | 2.0 ± 0.1 (7) | 1.9 ± 0.2 (6) | 1.9 ± 0.2 (7) |
| Recovery from fast inactivation (ms) | 238 ± 13 (8) | 236 ± 13 (6) | 237 ± 14 (7) | 314 ± 14 (6)** | 412 ± 16 (8)** | 360 ± 17 (9)** |
| Recovery from deep inactivation (ms) | 502 ± 27 (7) | 503 ± 13 (7) | 525 ± 22 (8) | 469 ± 13 (6) | 569 ± 20 (8)* | 557 ± 21 (7) |

[a]Weighted $\tau$.
Statistically significant differences are noted if the *P* value was $<0.05$ (*) or $<0.01$ (**). Data are expressed as mean values ± S.E.M. The number of cells is presented in parentheses.

above threshold, but were faster at more depolarized potentials, approaching a plateau above −10 mV (Fig. 3C). The voltage-independent rate for the $Ca_v3.3a$, b, and c isoforms was ~4.5 ms, while all three Δ33 variants were slower, approaching 6.6 ms. The Δ33 variants of $Ca_v3.3a$ and b were 1.4-fold slower at all test potentials, while the Δ33 variant of $Ca_v3.3c$ showed a bigger difference at negative test potentials (Fig. 3D). The kinetics of inactivation were also voltage-dependent at negative voltages, but in this case the rate was voltage-independent above −30 mV (Fig. 3E). The inactivation rate for all variants was similar during test pulses to −50 mV, while at higher test potentials the $Ca_v3.3a$, b, and c variants approached a voltage-independent rate of 69 ms. In contrast, the inactivation kinetics for all three Δ33 variants were 1.5-fold slower (Fig. 3F), approaching a voltage-independent rate of 96 ms (Fig. 3E). Although the Δ33 deletion slowed activation and inactivation kinetics of the $Ca_v3.3a$, b, and c variants, these effects appear to be independent because they occur at different voltages.

The kinetics of channel closing, or deactivation, were measured using a two-step protocol. Although this protocol generates substantial currents, they were well clamped as evidenced by the rise time of the tail current (0.20 ± 0.01 ms, $n = 51$). As described previously [6,12], $Ca_v3.3$ channels close in a biexponential manner (Fig. 4A). At very negative repolarization potentials (< −100 mV) all the splice variants behaved similarly, closing with an apparent $\tau$ of 1 ms (Fig. 4B), while at less negative potentials $Ca_v3.3b$ and c channels closed more slowly than $Ca_v3.3a$. The $Ca_v3.3\Delta33a$ variant closed with similar kinetics as the a isoform, and similar results were obtained with the Δ33 variants of b and c (Table 1).

Voltage-gated $Ca^{2+}$ channels can inactivate at membrane potentials that are more negative than the apparent threshold for channel opening, indicating that channels can enter inactive states directly from closed states [15,16]. Since the Δ33 variants inactivated more slowly at potentials where channels can open, we also examined whether they inactivate more slowly from closed states. Development of inactivation was measured by holding the membrane potential at either −60 or −70 mV for varying durations, and available channels were tested with a depolarizing pulse to −30 mV (Fig. 4C). As reported previously [6], $Ca_v3.3a$ channels inactivated in a biexponential manner, and similar results were obtained with all variants (Table 1). Each variant also showed a similar voltage dependence in its steady-state inactivation (Fig. 4D; Table 1).

Recovery from inactivation allows T-type channels to generate rebound bursts [1]. To measure the recovery that might occur after a burst, we inactivated channels with a 0.5 s step to −30 mV (Fig. 4E). We also measured the recovery that might occur during an inhibitory postsynaptic potential that precedes a burst; channels were inactivated with a 20 s step to −60 mV then allowed channels to recover at −90 mV (Fig. 4F). In both cases the time course of recovery was monoexponential, with faster recovery from the short inactivating pulse to −30 mV (Table 1). The $Ca_v3.3a$, b, and c isoforms recovered with a similar time course, while all the Δ33 variants were slower (Fig. 4E; Table 1). In contrast, all variants recovered from the long pulse at −60 mV with a similar time course (Fig. 4F; Table 1).

We conclude that splice variation affects transitions between channel states, with little effect on the voltage dependence of these transitions. A recent study of the human exon 33 variants reached a similar conclusion [17]. In contrast to the present results, their Δ33 variant inactivated faster in *Xenopus* oocytes, and they found few kinetic differences when the channels were expressed in 293 cells. Since the distal carboxy-terminus modulates the effect of the Δ33 variation, differences between the studies might be ascribed to their use of a truncated channel (see [12]). Kinetic differences between $Ca_v3$ isoforms have been suggested to have profound physiological consequences for neuronal firing [5], such that $Ca_v3.3\Delta33$ var-

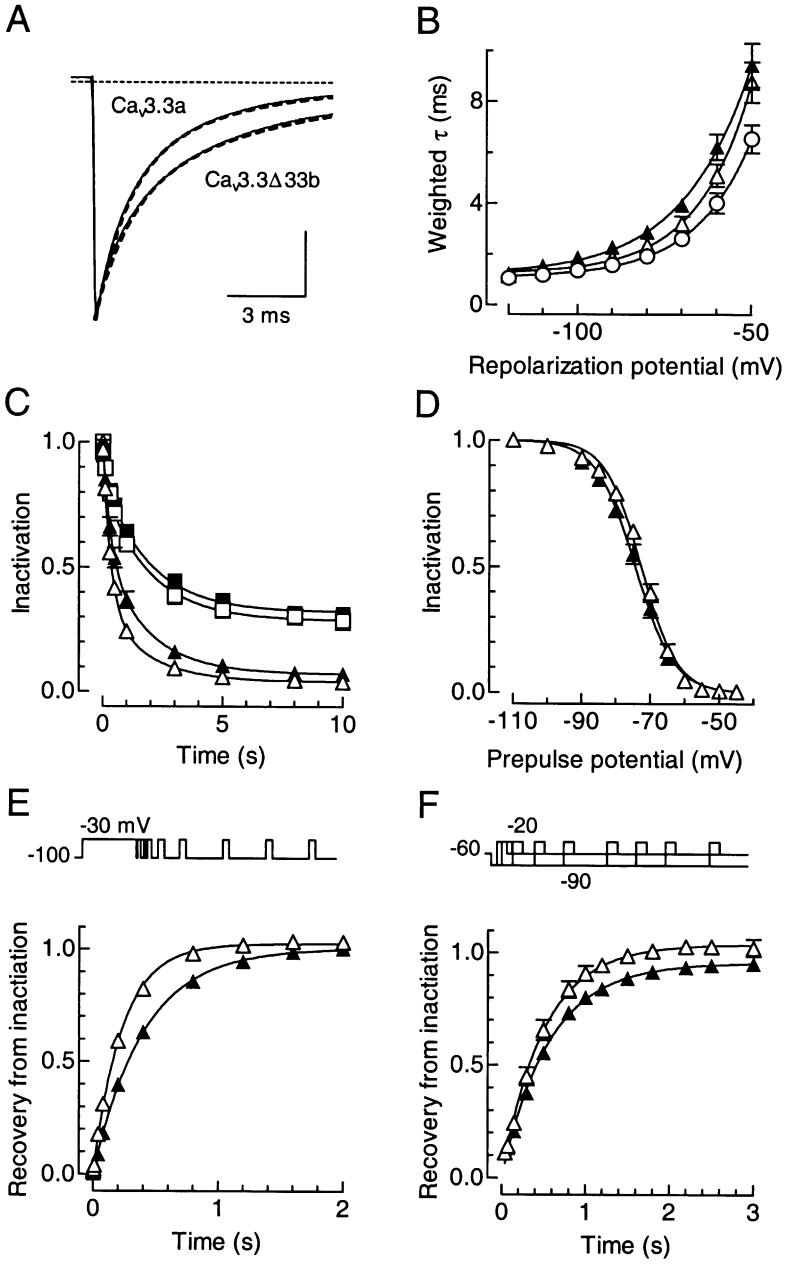


Fig. 4. Deactivation and inactivation kinetics of $Ca_v3.3$ channels. A: Representative tail currents evoked upon repolarization of the membrane to −70 mV after a 10 ms pulse to +60 mV. Dotted lines represent the fit of the tail current with two exponentials. Vertical scale bar: 4 nA for $Ca_v3.3a$, and 5.8 nA for $Ca_v3.3\Delta33b$. B: Deactivation kinetics. Points show the average weighted $\tau$ [12] at each repolarization potential for $Ca_v3.3a$ (○, $n=10$), $Ca_v3.3b$ (△, $n=8$), and $Ca_v3.3\Delta33b$ channels (▲, $n=10$). C: Development of inactivation. Cells expressing $Ca_v3.3b$ (open symbols) or $Ca_v3.3\Delta33b$ (closed symbols) were held at either −60 (△, ▲) or −70 mV (□, ■), for varying times, and then the available current was tested at −30 mV. D: Voltage-dependent steady-state inactivation. Channels were inactivated by a 15 s conditioning pulse to different potentials, then tested for channel availability with a 300 ms pulse to −30 mV. Each experimental data set was normalized to the peak current obtained after the −110 mV prepulse, then fit to a Boltzmann function. Average steady-state inactivation curves for $Ca_v3.3b$ (△, $n=9$) and $Ca_v3.3\Delta33b$ (▲, $n=7$) are shown. E: Recovery from fast inactivation. $Ca_v3.3b$ (△, $n=6$) and $Ca_v3.3\Delta33b$ (▲, $n=8$) channels were inactivated by a 500 ms pulse to −30 mV, and then channel availability was tested with a second pulse after an interpulse of variable duration. Recovery was defined as the ratio between the amplitude of the recovered current divided by the current elicited during the inactivating pulse. Channels were allowed to recover for 10 s between episodes. Each data set was fit with an exponential, and then averaged. F: Recovery from deep inactivation. $Ca_v3.3$ channels were inactivated by holding the membrane at −60 mV for 20 s, allowed to recover at −90 mV for variable times, then tested for recovery with a pulse to −20 mV. Average data sets from $Ca_v3.3b$ (△, $n=7$) and from $Ca_v3.3\Delta33b$ (▲, $n=8$) were fit with a single exponential.

iants with slower inactivation might give rise to more sustained firing patterns.

*Acknowledgements:* We thank Jennifer DeLisle for technical assistance. This work was supported by National Institutes of Health Grant NS38691 (to E.P.R.).

## References

[1] Huguenard, J.R. (1996) Annu. Rev. Physiol. 58, 329–348.
[2] Lee, J.H., Daud, A.N., Cribbs, L.L., Lacerda, A.E., Pereverzev, A., Klöckner, U., Schneider, T. and Perez-Reyes, E. (1999) J. Neurosci. 19, 1912–1921.
[3] McRory, J.E., Santi, C.M., Hamming, K.S., Mezeyova, J., Sutton, K.G., Baillie, D.L., Stea, A. and Snutch, T.P. (2001) J. Biol. Chem. 276, 3999–4011.
[4] Monteil, A., Chemin, J., Leuranguer, V., Altier, C., Mennessier, G., Bourinet, E., Lory, P. and Nargeot, J. (2000) J. Biol. Chem. 275, 16530–16535.
[5] Chemin, J., Monteil, A., Perez-Reyes, E., Bourinet, E., Nargeot, J. and Lory, P. (2002) J. Physiol. 540, 3–14.
[6] Frazier, C.J., Serrano, J.R., George, E.G., Yu, X., Viswanathan, A., Perez-Reyes, E. and Jones, S.W. (2001) J. Gen. Physiol. 118, 457–470.
[7] Huguenard, J.R., Gutnick, M.J. and Prince, D.A. (1993) J. Neurophysiol. 70, 158–166.
[8] Pan, Z.H. (2000) J. Neurophysiol. 83, 513–527.
[9] Tarasenko, A.N., Kostyuk, P.G., Eremin, A.V. and Isaev, D.S. (1997) J. Physiol. 499, 77–86.
[10] Huguenard, J.R. and Prince, D.A. (1992) J. Neurosci. 12, 3804–3817.
[11] Talley, E.M., Cribbs, L.L., Lee, J.H., Daud, A., Perez-Reyes, E. and Bayliss, D.A. (1999) J. Neurosci. 19, 1895–1911.
[12] Gomora, J.C., Murbartián, J., Arias, J.M., Lee, J.-H. and Perez-Reyes, E. (2002) Biophys. J. 83, 229–241.
[13] Mittman, S., Guo, J., Emerick, M.C. and Agnew, W.S. (1999) Neurosci. Lett. 269, 121–124.
[14] Bezanilla, F. (2000) Physiol. Rev. 80, 555–592.
[15] Patil, P.G., Brody, D.L. and Yue, D.T. (1998) Neuron 20, 1027–1038.
[16] Serrano, J.R., Perez-Reyes, E. and Jones, S.W. (1999) J. Gen. Physiol. 114, 185–201.
[17] Chemin, J., Monteil, A., Dubel, S., Nargeot, J. and Lory, P. (2001) Eur. J. Neurosci. 14, 1678–1686.